J Therm Anal Calorim (2012) 109:915–920
DOI 10.1007/s10973-011-1801-5

Effect of some metallic additives (Ag, Cd, and Sn) on thermal transport properties of a-Se

A. Sharma · K. Singh · N. Mehta

Received: 27 May 2011 / Accepted: 14 July 2011 / Published online: 30 July 2011

Abstract In this study, we have studied the effect of elements Ag, Cd, and Sn as chemical modifiers on some thermal transport properties (thermal conductivity, diffusivity, and specific heat per unit volume) of amorphous Se. Concurrent measurements of thermal transport properties such as effective thermal conductivity (λ_e), thermal diffusivity (χ_e), and specific heat per unit volume (ρC_v) are used at room temperature for twin pellets of pure Se- and Se-based binary $Se_{98}M_2$ (M = Ag, Cd, and Sn) alloys using transient plane source technique. We have also determined the thermal inertia I_T using the experimental values of thermal conductivity and specific heat per unit volume for present amorphous alloys. The increasing sequence of measured thermal transport properties is also discussed.

Keywords Thermal conductivity · Thermal diffusivity · Specific heat per unit volume · Thermal inertia · Transient plane source (TPS) technique

Introduction

The chalcogenide glasses as optical materials take one of the main places in the contemporary technologies. The success of engineer solutions in the different fields of the human activities depends on those that lead to more effective assimilation of these materials and to expansion of the spectra of their properties, as well as to purposeful searching of new materials with newer properties. The chalcogenide glasses are notably perspective and heightened interest on them is due to their relatively easy obtaining in the bulk and layered form [1–3]. They do not need deep purification and offer a wide range of possibilities for application. These materials have vast electrical, optical, and technological applications, such as in memory devices, optical fibers, Xerography, photolithography, infrared lenses, optical amplifiers, blue laser diodes, and solar cells [4–8]. These applications make them more attractive for their investigation. The modern technological applications of these materials such as image sensors, thermoelectric properties, and optical recording, have become possible due to recent improvements in preparation techniques. In the field of amorphous chalcogenide alloys, mostly selenium (Se)-based binary and ternary alloys are useful due to their greater hardness, high photosensitivity; higher crystallization temperature and smaller aging effect and low viscosity as compared to pure a-Se [9].

Ag-doped binary and ternary glasses are becoming important because some of them are used as materials for phase change optical storage (DVD disks, etc.). Although Se–Ag glasses and thin films exhibit a higher index of refraction, a red-shift absorption edge, and decreased sensitivity for alkaline etching as compared to pure a-Se. Conventionally Se–Ag glasses having many applications such as electrochemical sensors, photo-resists, optical waveguide, diffraction elements, Fresnel lenses, optical memories holography, and other optical and non-linear optical elements [10–15].

Cadmium selenide (Cd-Se) is the member of the family of group II and VI compounds and it is one of the best photo-conducting materials. It has potential applications in photo electrochemical solar cells, thin film transistor, and gamma ray detectors [16–19]. It has several applications in various nano-devices too like logic circuits, nano-sensors, and nano-thermometers.

A. Sharma · K. Singh · N. Mehta (✉)
Department of Physics, Banaras Hindu University, Varanasi 221005, India
e-mail: dr_neeraj_mehta@yahoo.co.in

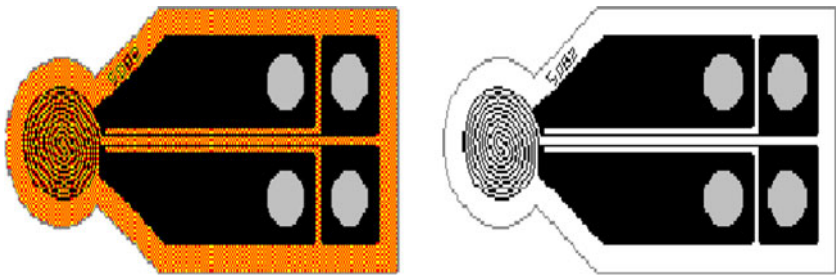

Fig. 1 Hot Disk sensors with Kapton insulation (*left*) for room temperature and Mica insulation (*right*) for extended temperature

Tin selenide (Se-Sn) has also potential applications such as in memory switching devices material and holographic recording system [20, 21]. The experimental value of absorption coefficient of Se–Sn alloys is $\sim 10^4$ cm^{-1} and the optical band gap vary from 1.03 to 1.4 eV by Imran [22]. The value of absorption coefficient makes tin-selenide glass suitable as a medium optical disk application, this optical band gap range of Se-Sn glass is close to the theoretical optimum for solar energy conversion and making for solar energy cell.

The addition of Ag, Cd, and Sn in a-Se may expand the glass-forming area and create compositional and configurationally disorder. The use of these binary chalcogenide glasses for industrial applications needs the alloys synthesized inexpensively. In order to make use of these materials in industrial applications, a better understanding of their thermo-physical properties is desirable [23, 24].

In this article, we have measured the results of effective thermal conductivity (λ_e), effective thermal diffusivity (χ_e), specific heat per unit volume (ρC_v) in a-Se and a-$Se_{98}M_2$ (M = Ag, Cd, and Sn) alloys. We have studied the effect of metallic additive (Ag, Cd, and Sn) on thermal transport properties of a-Se. We have also determined thermal inertia I_T by using experimental values of λ_e and ρC_v of present alloys. Results of these thermal transport parameters have been measured with help of transient plane source (TPS) technique introduced by Gustafsson [25].

Theoretical basis

One of the most precise and convenient techniques for studying thermal transport properties is the TPS method. It is a modern technique, yielding information on thermal conductivity, thermal diffusivity as well as specific heat per unit volume of the material under study.

The method is based on the use of a transiently heated plane sensor, and is in its most common adaptation referred to as the Hot Disk Thermal Constants Analyzer. The Hot Disk sensor consists of an electrically conducting pattern in the shape of a double spiral, which has been etched out of a thin metal (Nickel) foil. This spiral is sandwiched between two thin sheets of an insulating material (Kapton, Mica, etc.). The Hot Disk sensor of Kapton is used for room temperature while Mica sensors for extended room temperature. These sensors are shown in Fig. 1. When performing a thermal transport measurement, the plane Hot Disk sensor is fitted between two pieces of the sample each one with a plane surface facing the sensor. By passing an electrical current, high enough to increase the temperature of the sensor between a fraction of a degree up to several degrees, and at the same time recording the resistance (temperature) increase as a function of time, the Hot Disk sensor is used both as a heat source and as a dynamic temperature sensor.

The solution of the thermal conductivity equation is based on the assumption that the Hot Disk sensor is located in an infinite medium, which means that the transient recording must be interrupted as soon as any influence from the outside boundaries of the two sample pieces is recorded by the sensor. Typical sample sizes are between 1 and 10 cm^3 but can in special situations be reduced to 0.01 cm^3. The sample preparation is limited to the cutting of one plane surface on each one of the two sample pieces. From what is said above, it is important to note that the size of the flat sample surfaces should be appreciably larger than the diameter of the Hot Disk sensor in order to allow for not too short a transient recording.

To theoretically describe how the Hot Disk behaves, the thermal conductivity equation has been solved assuming that the Hot Disk consists of a certain number of concentric ring heat sources located in an infinitely large sample. If the Hot Disk is electrically heated, the resistance increase as a function of time can be given as

$$R(\tau) = R_0\{1 + \alpha[\Delta T_i + \Delta T_{ave}(\tau)]\} \quad (1)$$

where R_0 is the resistance of the disk just before it is heated or at time $t = 0$, α is the temperature coefficient of the resistivity, ΔT_i is the constant temperature difference that develops almost momentarily over the thin insulating layers which are covering the two sides of the Hot Disk sensor material (Nickel) and which make the Hot Disk a convenient sensor. $\Delta T_{ave}(\tau)$ is the temperature increase of the sample surface on the other side of the insulating layer and facing the Hot Disk sensor (double spiral). From Eq. 1, we get the temperature increase recorded by the sensor:

$$\Delta T_{\text{ave}}(\tau) + \Delta T_{\text{i}} = \frac{1}{\alpha}\left(\frac{R(t)}{R_0} - 1\right) \tag{2}$$

Here ΔT_{i} is a measure of the "thermal contact" between the sensor and the sample surface with $\Delta T_{\text{i}} = 0$ representing perfect "thermal contact" closely realized by a deposited (PVD or CVD) thin film or an electrically insulating sample. Figure 2 shows the curves of sensor and sample temperature in which the blue curve indicates the temperature increase of the sensor itself and the red one show how the temperature of the sample surface is increasing. Although ΔT_{i} becomes constant after a very short time Δt_{i} which can be estimated as

$$\Delta t_{\text{i}} = \frac{\delta^2}{\chi_{\text{e}}} \tag{3}$$

where δ is the thickness of the insulating layer and χ_{e} is the thermal diffusivity of the material, the time-dependent temperature increase is given by the theory as

$$\Delta T_{\text{ave}}(\tau) = \frac{P_0}{\pi^{3/2} a\, \lambda_{\text{e}}} D(\tau) \tag{4}$$

where P_0 is the total output of power from the sensor, a is the overall radius of the disk, λ_{e} is the thermal conductivity of the sample that is being tested, and $D(\tau)$ is a dimensionless time-dependent function which is given as

$$D(\tau) = \frac{1}{[m(m+1)]^2} \times \int_0^{\tau} \frac{\mathrm{d}\sigma}{\sigma^2}\left[\sum_{l=1}^{m} l\left\{\sum_{k=1}^{m} k \exp\frac{-(l^2+k^2)}{4\sigma^2 m^2} L_0\left(\frac{lk}{2\sigma^2 m^2}\right)\right\}\right] \tag{5}$$

with

$$\tau = \sqrt{\frac{t}{\Theta}} \tag{6}$$

where t is the time measured from the start of the transient recording and Θ is the characteristic time defined as

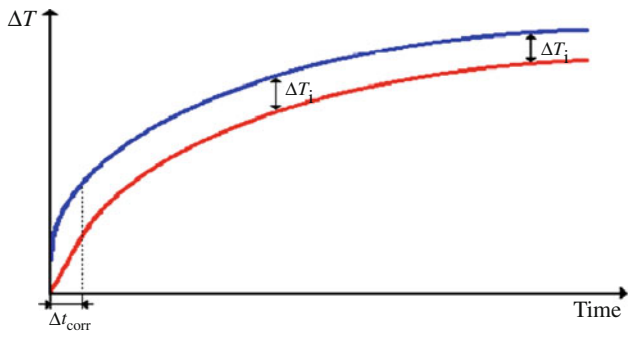

Fig. 2 Sensor and sample temperature increase curves

$$\Theta = \frac{a^2}{\chi_{\text{e}}} \tag{7}$$

where χ_{e} is the thermal diffusivity of the sample.

In Eqs. 4 and 5, P_0 is the total output power, L_0 is the modified Bessel function and l, k are the dimensions of the resistive pattern. To record the potential difference variations, which normally are of the order of a few milli-volts during the transient recording, a simple bridge arrangement as shown in Fig. 3 has been used. If we assume that the resistance increase will cause a potential difference variation $\Delta U(t)$ measured by the voltmeter in the bridge, the analysis of the bridge indicates that

$$\Delta E(t) = \frac{R_{\text{s}}}{R_{\text{s}} + R_0} I_0 \Delta R(t) = \frac{R_{\text{s}}}{R_{\text{s}} + R_0} \frac{I_0\, \alpha\, R_0 P_0}{\pi^{3/2} a\, \lambda} D(\tau) \tag{8}$$

Here

$$\Delta E(t) = \frac{\Delta U(t)}{[1 - C \cdot \Delta E(t)]} \tag{9}$$

and

$$C = \frac{1}{R_{\text{s}} I_0 \left[1 + \frac{\gamma R_{\text{p}}}{\gamma(R_{\text{s}}+R_0)+R_{\text{p}}}\right]} \tag{10}$$

The definition of various resistances is found in Fig. 3. R_{p} is the lead resistance, R_{s} is a standard resistance with a current rating that is much higher than I_0, which is the initial heating current through the arm of the bridge containing the TPS element and R_2 is variable resistance. γ is the ratio of the resistances in two ratio arms of the bridge circuit.

Now by making a computational plot of the recorded temperature increase versus D, we get a straight line, the

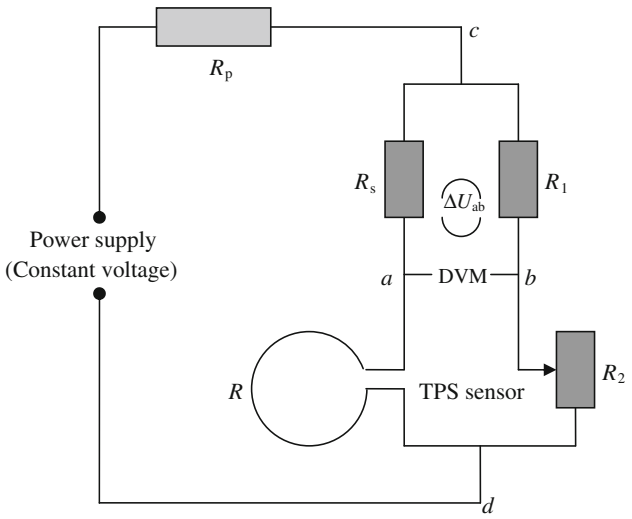

Fig. 3 Electrical circuit diagram used for simultaneous measurement of λ_{e}, χ_{e}, and ρC_{v}

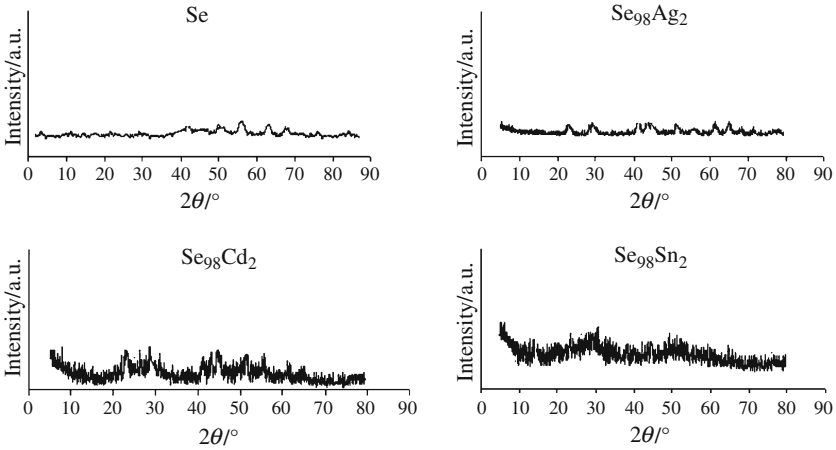

Fig. 4 XRD patterns of as-prepared a-Se and $Se_{98}M_2$ (M = Ag, Cd, and Sn) alloys

intercept of which is ΔT_i and the slope is $P_0/\pi^{3/2}a\ \lambda_e$ using experimental times much longer than Δt_i. Since λ_e and hence Θ are not known before the experiment, the final straight line from which the thermal conductivity is calculated is obtained through a process of iteration. Thus, it is possible to determine both the thermal conductivity and the thermal diffusivity from one single transient recording.

Experimental details

Material preparation

High purity (99.999%) selenium, silver, cadmium, and tin were weighed in appropriate proportions in quartz glass ampoules (length 5 cm and internal diameter (8 mm) to prepare a-Se and a-$Se_{98}M_2$ (M = Ag, Cd, and Sn) alloys. The content of each separate ampoule was sealed in a vacuum of 10^{-6} Torr and heated in a furnace where temperature was raised at a rate of 3–4 K min^{-1} up to 900 K and kept at that temperature for 10 h. The ampoules were frequently rocked to insure the homogeneity of the samples. The molten samples were then rapidly quenched in ice cooled water. The X-ray diffraction patterns of as-prepared samples were recorded using Philips PW-1700 powder diffractometer (operating at 20 keV) with Cu-K_α (λ = 1.54056 Å) radiation to confirm the glassy nature of alloys. The XRD patterns are shown in Fig. 4. Absence of any sharp peak confirms the amorphous nature of these samples.

Measurements of thermal transport properties

Ingots of the quartz ampoules were crushed into fine powder and then the pellets of thickness 2 mm and diameter 12 mm were prepared by a pressure machine. The pellets were made at a constant load of 5 tons and the surfaces of these pellets are smooth so as to insure perfect thermal contact between the samples and the heating elements, as the TPS sensor is sandwiched between the two pellets of sample material in the sample holder. Set-up of TPS technique is shown in Fig. 5. TPS technique in which a TPS element is made of 10 μm thick nickel foil with insulating a layer made of 50 μm thick kapton on each side of metal pattern. At the room temperature, computer operated TPS gives desired values of thermal transport

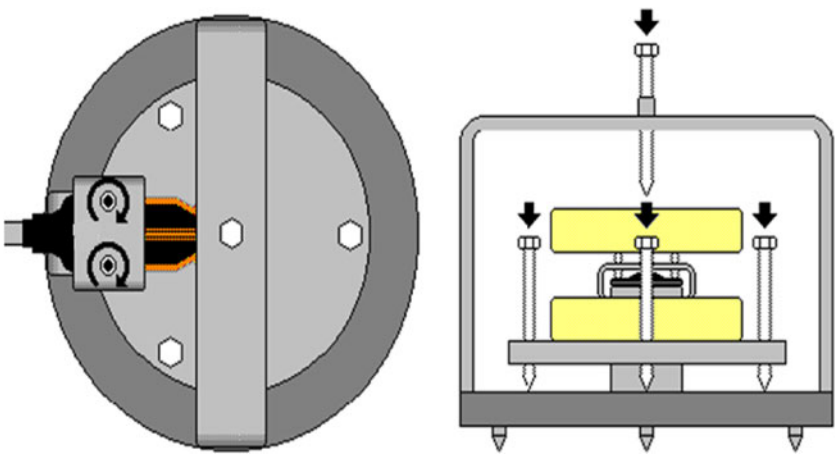

Fig. 5 Room temperature holder set-up of TPS technique

parameters like effective thermal conductivity (λ_e), effective thermal diffusivity (χ_e), and specific heat per unit volume (ρC_v) as shown in Fig. 5. Simultaneous measurements are done on thermal transport properties (effective thermal conductivity (λ_e) and effective thermal diffusivity (χ_e), specific heat per unit volume (ρC_v) in pellets of a-Se and a-$Se_{98}M_2$ (M = Ag, Cd, and Sn) alloys. The pellets were compressed under constant load of 5 tons were carried out, at room temperature using TPS technique.

Results and discussion

The solution of the thermal conductivity equation is based on the assumption that the sensor is located in an infinite material which means that the total time of the transient recording is limited by the presence of the outside boundaries or the limited size of the sample. In other words, the "thermal wave" or "thermal penetration depth" generated in an experiment must not reach the outside boundaries of the sample pieces during the transient recording. An estimation of how far this thermal wave has proceeded in the sample during a recording is the so-called probing depth, defined as

$$\Delta_p = 2\sqrt{t\lambda_e} \tag{11}$$

where t is the measuring time of the experiment and the constant 2 has been determined so that the influence of external sample boundaries on the temperature of the sensor cannot be detected when the probing depth Δ_p is limited to within the sample boundaries. A consequence of this equation is that the distance from any point of the sensor to any point on the surface of the two sample pieces must exceed Δ_p if the total measuring time is t. The relation between the probing depth and the total measuring time of the experiment indicates that it is easier to make measurements on larger samples. In order to determine both the thermal conductivity and thermal diffusivity with good accuracy, the thickness of a flat sample should not be less than the radius of the hot disk sensor.

The values of λ_e, χ_e, and ρC_v for a-Se and a-$Se_{98}M_2$ (Ag, Cd, and Sn) alloys are shown in Table 1. We have also determined thermal inertia I_T of these alloys using the expression (12):

$$I_t = \sqrt{\rho C_v \lambda_e} \tag{12}$$

The values of I_T are also given in Table 1. From this table it is clear that the increasing sequence of all the thermal transport properties in binary alloys is ($Se_{98}Sn_2$) < ($Se_{98}Cd_2$) < ($Se_{98}Ag_2$). This clearly shows that Ag plays the better role of chemical modifier as compared to other two additives, since it may produce large changes in thermal conductivity, thermal diffusivity, specific heat per unit volume, and thermal inertia in pure a-Se.

Table 1 Thermal transport properties (λ_e, χ_e, ρC_v, and I_T) of a-Se and $Se_{98}M_2$ (M = Ag, Cd, and Sn) alloys

Sample	λ_e/ W m^{-1} K^{-1}	χ_e/ mm^2 s^{-1}	ρC_v/ MJ m^{-3} K	I_T/kJ m^{-2} K^{-1} $s^{1/2}$
a-Se	0.2	0.075	2.67	0.7307
$Se_{98}Ag_2$	0.325	0.2555	1.274	0.6435
$Se_{98}Cd_2$	0.2937	0.2548	1.153	0.5821
$Se_{98}Sn_2$	0.2661	0.2453	1.084	0.5372

The observed results can be explained on the basis of the thermal conductivity and specific heat per unit volume of Ag, Cd, and Sn additives. The increasing order of these values is Sn < Cd < Ag which is similar to the increasing sequence observed in binary alloys. As these elements are mixed in similar proportion (2 at%) in pure a-Se so the above increasing order in thermal conductivity and specific heat of additives Ag, Cd, and Sn is probably responsible for the presents results.

It is also reported in literature by Mehta et al. [26] that the decrease in density of localized states increases the porosity of alloys which is responsible for decrease of effective thermal conductivity, effective thermal diffusivity, and specific heat per unit volume. In our case also, the increasing sequence of density of additive elements is Ag < Cd < Sn. This is another appropriate reason for high values of thermal transport properties in case of $Se_{98}Ag_2$ alloy as compared to $Se_{98}Cd_2$ and $Se_{98}Sn_2$.

Conclusions

The effect of silver, cadmium, and tin on thermal transport properties such as thermal conductivity, thermal diffusivity, specific heat per unit volume, and thermal inertia of a-$Se_{98}M_2$ alloys have been studied. The major conclusions are as follows:

(a) The results indicate that the values of thermo-physical parameters measured in the present study are high for $Se_{98}Ag_2$ alloy as compared to $Se_{98}Cd_2$ and $Se_{98}Sn_2$ alloys. This indicates that Ag as a chemical modifier affects more significantly the thermo-physical properties of a-Se.

(b) The increasing sequence of thermal transport parameters in binary alloys is explained on the basis of thermal conductivity and specific heat per unit volume of Ag, Cd, and Sn additives.

(c) The decreasing sequence of density of additive elements (Ag, Cd, and Sn) is just opposite to that of thermal transport properties of corresponding binary alloys.

Acknowledgements The authors (NM and KS) are thankful to UGC, New Delhi, India for providing equipment grant to purchase TPS unit under UGC networking program.

References

1. Marquez E, Gonzalez-leal JM, Prieto-alcon R, Vlcek M, Stronski A, Wagner T, Minkov D. Optical characterization of thermally evaporated thin films of $As_{40}S_{40}Se_{20}$ chalcogenide glass by reflectance measurements. Appl Phys A. 1998;67:371–8.
2. Takeuchi H, Matsuda O, Murase K. Reversible mesoscopic structural transformations in vacuum evaporated amorphous $Ge_{30}Se_{70}$ film studied by Raman scattering. J Non-Cryst Solids. 1998;238:91–7.
3. Rajagopalan T, Reddy GB. Study of surface topography and optical properties of $Ge_{15}Bi_{38}Se_{47}$ films. J Mater Sci. 1998;9:133–7.
4. Adler D. Amorphous semiconductors devices. Sci Am. 1977;236:36–48.
5. Dessaur JH, Clark HE. Xerography and related processes. London: Focal Press; 1965.
6. Savage JA, Webber PJ, Pitt AM. The potential of Ge–As–Se–Te glasses as 3–5 μm and 8–12 μm infrared optical materials. IR Phys. 1980;20:313–20.
7. Trnovcona V, Furar I, Lezal D. Influence of doping on physical properties of vitreous As_2Se_3. J Non-Cryst Solids. 2007;353:1311–3.
8. Goyal N, Zolanvari A, Tripathi SK. Effect of silver dissolution on electrical properties of As_2S_3. J Mater Sci. 2001;12:523–6.
9. Kotkata MF, El-Mousy MK. A survey of amorphous Se–Te semiconductors and their characteristic aspects of crystallization. Acta Phys Hung. 1983;54:303–12.
10. Shimkawa K, Kolobov AV, Elliot SR. Photo-induced effects and meta-stability in amorphous semiconductors and indulators. Adv Phys. 1995;44:475–588.
11. Aniya M. A model for the anomalous electronic properties in liquid silver chalcogenides: implications from a viscoelastic theory. J Therm Anal Calorim. 2010;99:109–15.
12. Kolobov AV, Tanaka K. Photo induced phenomena in amorphous chalcogenide: from phenomenology to nano scale. In: Nalwa HS, editor. Hand book of advanced electronic and photonic materials and devices, vol 5. New York: Academic Press; 2001. p. 47–90.
13. Kawaguchi T, Tanaka K, Elliott SR. Photo induced and electron beam phenomena in Ag-rich amorphous chalcogenide semiconductors. In: Nalwa HS, editor. Hand book of advanced electronic and photonic materials and devices, vol 5, chalcogenide glasses and sol–gel materials. New York: Academic Press; 2001. p. 91–117.
14. Popescu MA. Non-crystalline chalcogenides. Dordrecht: Kluwer Academic Publishers; 2000.
15. Mitkova M. Real time optical recording on thin films of amorphous semiconductors. In: Boolchand P, editor. Insulating and semiconducting glasses. Singapore: World Scientific Publishers; 2000. p. 814–43.
16. Wagner T, Frumar M. Optically induced diffusion and dissolution of metals in amorphous chalcogenide. In: Kolobov AV, editor. Photo induced metastability in amorphous semiconductors. Berlin: Wiley-VCH Verlag; 2003. p. 196–216.
17. Rajpure KY, Anarase PA, Lokhande CD, Bhosale CH. Photoelectrochemical studies on electrodeposited Cd-Fe Se thin films. Phys Status Solidi. 1999;172:415–23.
18. Dhumure SS, Loknande CD. Studies on photo-electrochemical storage cells formed with chemically deposited CdSe and Ag_2S electrodes. Sol Energy Mater Sol Cells. 1993;29:183–94.
19. Froment M, Cachet H, Essaaidi H, Maurin G, Cortes R. Metal chalcogenide semiconductors growth from aqueous solutions. Pure Appl Chem. 1997;69:77–82.
20. Min S-K, Joo O-S, Mane RS, Jung K-D, Lokhande CD, Han S-K. CdSe nano-fiber based photo-electrochemical cells: Influence of annealing temperatures. J Photochem Photobiol A. 2007;187:133–7.
21. Baxter CR, Mclennan WD. Ovonic type switching in selenide thin films. J Vac Sci Technol. 1975;12:110–3.
22. Bennouna A, Tessier PY, Priol M, Dang Tran Q, Robin S. Far ultraviolet photoelectric study of thin SnSe evaporated films. Phys Status Solidi (B). 1983;117:51–6.
23. Saraswat S, Kushwaha SSS. Specific heat studies in a-Se and a-$Se_{90}M_{10}$ (M = In, Sb, Te) alloys. J Therm Anal Calorim. 2009;96:923–7.
24. Albright G, Farid M, Al-Halla S. Development of a model for compensating the influence of temperature gradients within the sample on DSC-results on phase change materials. J Therm Anal Calorim. 2010;101:115–1160.
25. Gustafsson SE. Transient plane source techniques for thermal conductivity and thermal diffusivity measurements of solid materials. Rev Sci Instrum. 1991;62:797–804.
26. Mehta N, Singh K, Saxena NS. Effect of In and Zn additives on some thermal properties of a-Se. Solid State Sci. 2010;12:963–5.